Phase diagram, stability and electronic properties of an Fe−P system under high pressure: a first principles study†

Ziyuan Zhao,[a] Lulu Liu,[a] Shoutao Zhang,[a] Tong Yu,[a] Fei Li[a] and Guochun Yang*[ab]

Fe−P binary compounds have attracted much attention, particularly under high pressure, since they are the constituents of the Earth's core. However, most studies focus on the single stoichiometry of Fe−P binary compounds at high pressure, and their whole phase diagram and relative stabilities have been unexplored thus far. Herein, first principles swarm structure predictions are performed to find stable structures of Fe−P compounds with various Fe_xP_y ($x = 1–4$ and $y = 1$, or $x = 1$ and $y = 2$) compositions. Then, their phase diagram and relative stabilities are reliably determined based on predicted structures. Specifically, the FeP, Fe_2P and Fe_4P compounds are found to be stable in the pressure range of 0–400 GPa. The Fe_3P compound decomposes into Fe_2P and Fe_4P above 214 GPa. FeP_2 becomes unstable above 82 GPa. Notably, two new phases (*i.e.* $C2/c$-structured Fe_4P and *Cmcm*-structured Fe_3P) are found to be more stable than the previously reported phases. In addition, the XRD pattern of the predicted *Cmcm*-structured Fe_3P matches the experimental patterns, and we are awaiting future experimental confirmation. Electronic band calculations show that the Fe−P binary compounds are metallic, with a pronounced Fe 3d component crossing the Fermi level. *Cmcm*-structured Fe_3P is ferromagnetic. Our study not only provides useful information for the further study of Fe−P binary compounds but also for the determination of the Earth's core components.

1. Introduction

Geochemical and geophysical studies show that light elements (*i.e.* hydrogen, oxygen, carbon, sulfur, phosphorus and silicon) play important roles in the Earth's core.[1,2] Early models of the Earth's core consisted of a considerable amount of schreibersite, cohenite, and troilite.[3] The Fe content of the Earth's core is rather rich (90.67%).[3] Several phases of iron compounds, such as iron–sulfur, iron–silicon, and iron–oxygen, with light elements under high pressure have been determined by a large number of experimental and theoretical studies.[4–7] Notably, the phosphorus content of the Earth's core was estimated to be around 0.20 wt%, and up to 4 wt% of phosphorus was found to be soluble in crystalline iron at 23 GPa in the Fe–S–P system.[8,9] Since the structures of Fe–P compounds are similar to that of

Fe–S, iron phosphides should have a stable composition in the cores. As a consequence, investigation of the structures and properties of iron-phosphorus (Fe–P) compounds is worthy of attention.

To date, extensive studies have been carried out on Fe–P binary compounds, and although most of these studies were based on single stoichiometry, the relative stabilities of the Fe–P binary compounds remain undetermined, particularly at high pressure. For example, several stoichiometric compounds (*i.e.* Fe_4P, Fe_3P, Fe_2P, FeP and FeP_2) were separately investigated. Fe_4P is known as melliniite, which is a mineral from Northwest Africa 1054 acapulcoite. The cubic polymorph with the $P2_13$ space group symmetry ($AlAu_4$-type structure) was determined using single-crystal X-ray diffraction data (XRD).[10] Under high pressure, the Fe_4P phase is relatively stable compared to Fe_3P + Fe.[11] The tetragonal structure Fe_3P was discovered from schreibersite at ambient pressure.[12] Its possible high-pressure polymorph is either a $P4/mnc$ or $Pnma$ structure, as predicted by theoretical calculations, and the pressure-induced phase transition from $I\bar{4}$ to $P4/mnc$ has been observed at 64 GPa.[13] For the Fe_2P compound, it is a terrestrial garnet peridotite with implications for the Earth's core. A hexagonal structure of Fe_2P with $P\bar{6}2m$ symmetry exists at ambient conditions, and the Co_2Si-type structure (space group *Pnma*) is found to be more stable above 8.0 GPa (ref. 14) or 16.8 GPa,[15] as observed through high-pressure and high-temperature X-ray diffraction experiments. Based on first principles calculations,

ᵃCentre for Advanced Optoelectronic Functional Materials Research and Laboratory for UV Light-Emitting Materials and Technology of Ministry of Education, Northeast Normal University, Changchun 130024, China. E-mail: yanggc468@nenu.edu.cn

ᵇState Key Laboratory of Superhard Materials, Jilin University, Changchun 130024, China

† Electronic supplementary information (ESI) available: Pressure phase diagram of the elementary substances of Fe and P; the calculated enthalpy difference as a function of pressure, for the reaction equation: $2Fe_3P \leftrightarrow Fe_2P + Fe_4P$; enthalpy differences of the Fe_3P and Fe_4P compounds as a function of pressure; calculated phonon spectra for the Fe_3P and Fe_4P compounds; calculated ICOHPs of Fe–Fe, and Fe–P pairs in Fe_4P. See DOI: 10.1039/c7ra01567d

another $P\bar{3}m$-structured Fe_2P was reported at 153 GPa.[16] Several studies on FeP have been carried out because FeP is also an important member in the planetary cores. FeP crystallizes in the regular MnP-type structure (space group $Pnma$) at ambient conditions and undergoes a structural phase transition to a simple cubic FeSi-type phase (space group $P2_13$) at 87.5 GPa.[17,18] FeP_2 crystallizes in the regular marcasite structure (space group $Pnnm$) at ambient conditions with no unpaired spins in the low-spin configuration.[19] Under high-pressure and high-temperature conditions, a new phase of FeP_2 with $I4/mcm$ symmetry was observed at 70 GPa.[20] Recent studies show that Fe–P binary compounds (*i.e.* Fe_3P, Fe_2P, FeP, FeP_2 and FeP_4) are stable at ambient pressure,[21] in which all the structures came from reported compounds. By all appearance, it is necessary to establish the whole phase diagram of Fe–P binary compounds under high pressure.

Recently, the first principles structural prediction method has become an irreplaceable tool to discover new materials and determine their stable structures.[22–24] For example, a recent breakthrough in the superconductivity field is the observation of remarkably high superconductivity (with T_c up to 203 K),[25] in which H_3S is the main stoichiometry of the superconducting phase.[26] This observation was achieved by direct investigation on the theoretical prediction of high-T_c superconductivity in compressed solid H_2S.[27] A new clathrate sodalite-like BN structure was predicted with a high energy density and large hardness.[28] The reaction of iron with xenon has been predicted in the Earth's inner core environment through theoretical calculations, which provides a solution to the missing Xe paradox.[29] Numerous unusual stoichiometric compounds with exotic physical or chemical properties have been discovered under high pressure.[30–37]

Herein, the most stable structures of the Fe–P binary compounds (Fe_4P, Fe_3P, Fe_2P, FeP and FeP_2) are reliably determined using the first principles calculations in combination with the swarm structural search technology.[23,38] The relative stabilities of these considered compounds are reliably established. Two new phases ($C2/c$-structured Fe_4P, and $Cmcm$-structured Fe_3P) are found to be more stable than the previously reported phases. $Cmcm$-structured Fe_3P meets the Stoner criterion and is ferromagnetic. Our study provides some useful information for the investigation of the constituents of the Earth's core.

2. Computational details

To search the stable structures for the given chemical compositions, structural predictions of the Fe–P system were performed at 0, 50, 100, 200, 300, and 400 GPa using the Crystal structure AnaLYsis by the Particle Swarm Optimization (CALYPSO) code.[23,39] The CALYPSO method can successfully find stable structures just depending on chemical compositions and has demonstrated success in predicting the high-pressure structures of various systems.[40–44] The *ab initio* structural relaxations and electronic calculations are based on the density functional theory (DFT) within the Perdew–Burke–Ernzerhof (PBE) of the generalized gradient approximation (GGA),[45] as implemented in the Vienna *ab initio* simulation package (VASP) code.[46] The electron–ion interaction was described using the all-

electronic projector-augmented wave (PAW) method[47] with $3s^23p^63d^74s^1$ and $3s^23p^3$ valence electrons for the Fe and P atoms, respectively. Hubbard U is necessary to correct the effective on-site electron–electron interaction of the transition metal, with valence electrons on the d and f orbits.[48,49] Hubbard U parameters with $U = 2$ eV and $J = 0.95$ eV were applied to the Fe atoms in the Fe_2P compounds.[16] It successfully reproduces the experimental magnetic moments of Fe atoms.[50] As a consequence, we chose Hubbard U with 2 eV at a fixed value of 0.95 eV (*i.e.* $U_{eff} = U - J$) to calculate the properties and fine structure optimization. $U = 2.2$ eV was verified to be suitable to elemental iron by the linear response approach.[51] The cutoff energy of 700 eV and Monkhorst–Pack[52] k-meshes with a grid spacing of $2\pi \times 0.03$ Å^{-1} were used to ensure that the total energy calculations converged well. The phonon calculations were carried out using the finite displacement approach to determine the dynamical stability of the predicted structures, as implemented in the Phonon code.[53] To study the interatomic interaction, the integrated crystal orbital Hamilton populations (ICOHPs) were calculated as implemented in the LOBSTER package.[54]

3. Results and discussion

3.1. Phase stabilities of Fe–P compounds

Herein, we mainly considered Fe-rich phosphorus compounds (*i.e.* Fe_4P, Fe_3P, Fe_2P, FeP and FeP_2) since the Fe content of the Earth's core is estimated to be around 90.67% and P content is about 0.17%.[3] In this study, the pressure ranges up to 400 GPa are considered. The predicted structures of Fe–P binary compounds were used to evaluate the formation enthalpy (ΔH) relative to the elemental solids Fe and P according to eqn (1), in order to explore the thermodynamic stabilities of Fe–P compounds.

$$\Delta H(Fe_mP_n) = [H(Fe_mP_n) - mH(Fe) - nH(P)]/(m + n),$$
$$(m = 1–4 \text{ and } n = 1, \text{ or } m = 1 \text{ and } n = 2) \quad (1)$$

where $H = U + PV$ is the enthalpy of each composition and ΔH is the enthalpy of formation per atom. Herein, U, P, and V are the internal energy, pressure, and volume, respectively. The relative stabilities of the considered compositions at the selected pressures of 0, 50, 100, 200, 300, and 400 GPa, with ΔH evaluated per atom, are shown in Fig. 1a. The stable phase lies on the convex hulls (the global stability lines). As can be seen, all the considered compositions are stable at 0 GPa, which is well in agreement with the recent theoretical study.[21] It should be noted that the Fe_4P compound is not included in the study by Jing Wu *et al.*[21] $P2_13$-structured Fe_4P has been found from melliniite and is confirmed to be stable at ambient pressure.[10] The known Fe_4P, Fe_3P, Fe_2P, FeP, and FeP_2 structures[10,17,19,55,56] at ambient pressure were well reproduced in our calculations, which validates our structure searching method applied to the Fe–P system. In addition, our calculated lattice parameters for Fe_3P (space group $I\bar{4}$, 8 formula units per cell) are $a = b = 9.13$ Å and $c = 4.40$ Å, which are in excellent agreement with the experimental values at $a = b = 9.10$ Å and $c = 4.46$ Å.[12] These lattice parameter calculations support the validity of the pseudo potentials adopted in this study.
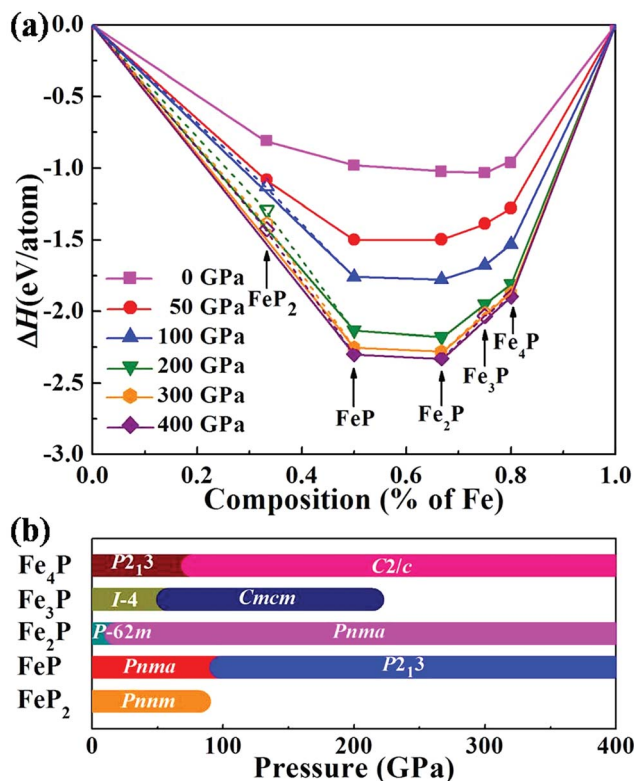
(a) Convex hulls figure

Fig. 1 Relative thermodynamic stabilities of Fe–P compounds. (a) Convex hulls of the calculated formation enthalpy per atom of the Fe–P system relative to the elemental solids Fe and P are shown as solid lines. Compounds corresponding to data points located on the convex hulls are thermodynamically stable. The *bcc* structure,[57] and *hcp* structure[58] of solid Fe, and the phases I (*Cmca*), II (*Pm3̄m*), III (*P6/mmm*), IV (*Im3̄m*), and V (*I4̄3d*) of solid P[59,60] are used to calculate the enthalpy of formation. Detailed information about the element solids can be found in Fig. S1.† (b) Pressure–composition phase diagram of the Fe–P system.

Under high pressure, the relative stabilities of our considered compositions are significantly different from that at ambient pressure. Specifically, the FeP_2 compound becomes unstable above 82 GPa, whereas the iron-rich compounds are relatively stable under high pressure. These phases of Fe_4P, Fe_2P and FeP are stable in the entire considered pressure range (0–400 GPa). Notably, the Fe_3P phase is unstable compared above 214 GPa (Fig. S2†) and decomposes into Fe_2P plus Fe_4P. The pressure–composition phase diagram of the Fe–P system is shown in Fig. 1b. For all the predicted structures, the calculated phonon dispersion curves confirm their dynamical stability with no imaginary frequencies observed in the entire Brillouin zone (Fig. S4†).

3.2. Geometry structure of the stable phases

Two new phases (*i.e.* $C2/c$-structured Fe_4P and *Cmcm*-structured Fe_3P) were discovered by comparing previous structures and our predicted structures, and their structural characters are shown in Fig. 2. The predicted $C2/c$-structured Fe_4P (4 formula units) is more stable than the phase with $P2_13$ symmetry above 37 GPa (Fig. S3a†). Its lattice parameters are $a = 7.342$ Å, $b = 3.772$ Å
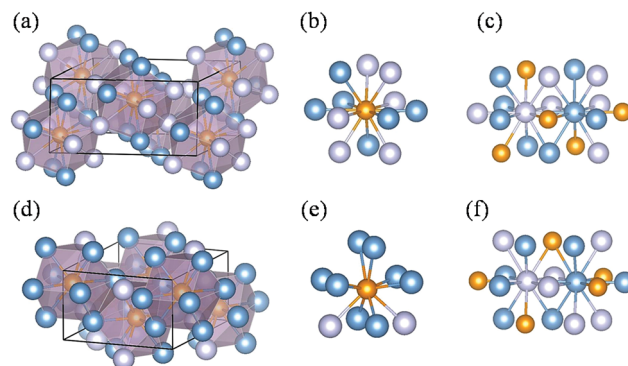

Fig. 2 Crystal structures of the Fe_4P and Fe_3P compounds at 200 GPa. (a) Fe_4P in the $C2/c$ structure. (b) Coordination environment of the P atom in Fe_4P. (c) Coordination environment of the Fe atoms in Fe_4P. (d) Fe_3P in the *Cmcm* structure. (e) Coordination environment of the P atom in Fe_3P. (f) Coordination environment of the Fe atom in Fe_3P. Here, the large shallow blue or dark blue and small orange spheres represent Fe and P atoms, respectively.

and $c = 5.627$ Å at 200 GPa. The structure contains two inequivalent Fe atoms occupying 8f (0.297, 0.337, 0.850) and 8f (0.900, 0.671, 0.551) sites and one equivalent P atom sitting at the 4e (0.000, 0.170, 0.750) position (Fig. 2a). To distinguish the two Fe atoms at different sites, we labelled the inequivalent Fe atoms with two different colors (Fig. 2c). In this structure, each P atom is in 12-fold coordination with the Fe atoms (Fig. 2b), forming a tetrakaidecahedron. The adjacent polyhedrons are interconnected through common edges or co-vertices. The distance of the two nearest Fe–Fe is 2.11 Å, which is smaller than the Fe–Fe distance of 2.48 Å in bulk Fe with $Im3̄m$ symmetry under ambient conditions[57] and 2.44 Å in Fe_2SH_3 at 100 GPa.[43] However, this structure is nonmagnetic, as will be discussed later. To determine the interatomic interaction in the $C2/c$-structure Fe_4P, the integrated crystal orbital Hamilton populations (ICOHPs) for the Fe–P and Fe–Fe.

Pairs at 200 GPa were calculated and are shown in Table S1.† The values of ICOHP between the Fe–P and Fe–Fe pairs are −1.80 and −4.97 eV, respectively. The ICOHP value of the Fe–Fe pair is very close to −4.90 eV in Fe_2SH_3.[43] Apparently, the Fe–Fe interaction plays an important role in determining the structural stability of the compound. Further analysis indicates that the major contribution of the Fe–Fe interaction originates from 4s–3d, which corresponds to the decomposed ICOHP of −1.908 eV per pair.

The Fe_3P compound with the $I4̄$ structure symmetry is stable at ambient conditions, and the first phase transition is observed at 64 GPa.[13] This phase is assigned as the $P4/mnc$ or *Pnma* structure. Notably, we discovered an orthorhombic structure of Fe_3P (space group *Cmcm*, 4 formula units per cell) above 58 GPa. This structure is much more stable than the $P4/mnc$ or *Pnma* structure in the pressure range of 0–400 GPa (Fig. S3b†). The lattice parameters of the *Cmcm*-structure Fe_3P are $a = 5.446$ Å, $b = 6.569$ Å and $c = 3.255$ Å. This structure contains two inequivalent Fe atoms occupying the 4c (0.500, 0.900, 0.750), and 8g (0.784, 0.117, 0.750) positions, and one equivalent P occupying the 4c (0.000, 0.170, 0.250) site. For each P atom, there are 10
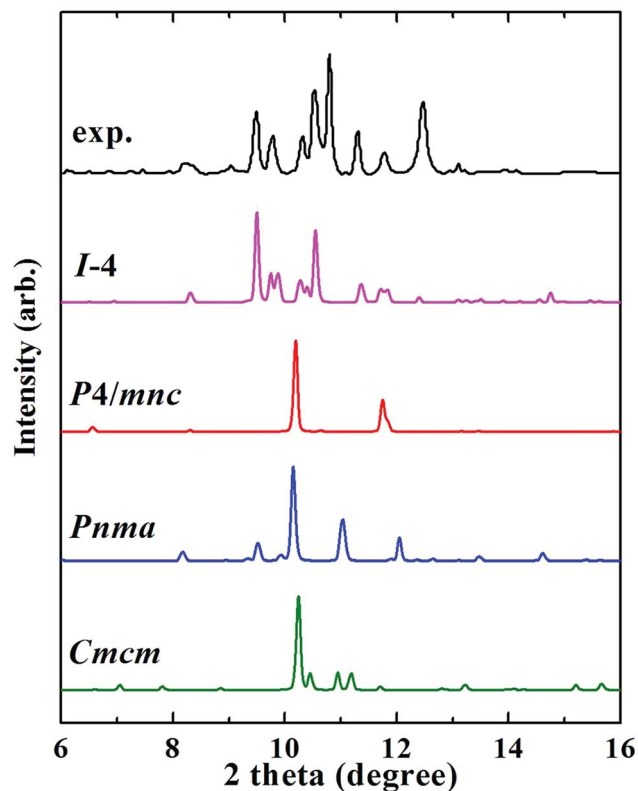
Fig. 3 XRD patterns of Fe$_3$P selected in synchrotron X-radiation with a fixed wavelength of 0.3344 Å at 64 GPa. The XRD pattern of Fe$_3$P is described by a black line, which was collected in an experimental work.[13] The XRD patterns of *I4*, *P4/mnc*, *Pnma*, and *Cmcm* structures are labelled by pink, red, blue, and green lines, respectively.

Fig. 4 Electronic band structures and projected density of states (PDOS) of the *C2/c*-structured Fe$_4$P (a and b), and the *Cmcm*-structured Fe$_3$P (c and d). The electronic band structures of spin up and spin down are described by the black and green lines, respectively.

nearest neighbours of Fe atoms, forming a P–Fe hendecahedron (Fig. 2e). The adjacent polyhedrons have common edges. The two inequivalent Fe atoms are labelled with two different colors (Fig. 2f). The nearest Fe–Fe distance in the *Cmcm* phase is 2.10 Å, which is comparable to 2.14 Å in Fe$_4$P. Unlike Fe$_4$P with *C2/c* symmetry, the *Cmcm*-structured Fe$_3$P structure is magnetic. An experimental study investigated the phase transitions of Fe$_3$P, in which the *P4/mnc* or *Pnma* structure is stable above 64 GPa.[13] However, our predicted *Cmcm* phase is more stable than the *P4/mnc* or *Pnma* phase at 64 GPa. The specific ΔH values of the three Fe$_3$P phases can be found in Table S2.† To confirm the existence of the *Cmcm* phase, the simulated XRD pattern of the *Cmcm* phase is shown in Fig. 3 along with the experimental patterns. Several possible structures of Fe$_3$P are also included in Fig. 3. Clearly, the main peak of *Cmcm*-structured Fe$_3$P is close to the experimental peaks or that of the other phases. Thus, *Cmcm*-structured Fe$_3$P might disappear under these experimental conditions.

3.3. Electronic properties of stable phases

The electronic band structures and projected density of states (PDOS) of the Fe$_4$P and Fe$_3$P compounds are shown in Fig. 4. Similar to the electronic properties of the other Fe–P species,[18] there are several bands crossing the Fermi level, which indicate that they are metallic. As can be seen in Fig. 4, there is
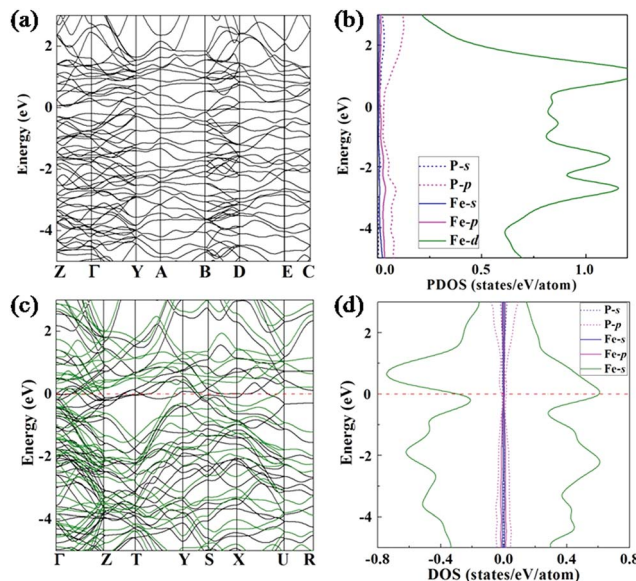
a common character of a pronounced Fe 3d component near the Fermi level. Interestingly, the *Cmcm*-structured Fe$_3$P is a ferromagnetic phase with the magnetic moment of 3.31μ_B per cell at 200 GPa by our calculations. Its electronic band structures and spin-polarized DOS based on spin up and spin down can be found in Fig. 4c and d. The calculated DOS per Fe atom at the Fermi level is about 1.0 eV^{-1} (Fig. 4d), which satisfies the Stoner criterion.[61]

4. Conclusion

To find the stable phases of Fe–P binary compounds, we explored the crystal structures and stabilities of the Fe–P system with Fe$_x$P$_y$ ($x = 1$–4 and $y = 1$, or $x = 1$ and $y = 2$) compositions under high pressure using first principles calculations combined with swarm structural searches. It is found that the FeP, Fe$_2$P and Fe$_4$P compounds are stable in the whole pressure range of 0–400 GPa, and Fe$_3$P becomes unstable above 214 GPa. Several phases of iron-rich compounds can be synthesized at elevated conditions, which may be the possible phases in the Earth's cores. The Fe$_4$P and Fe$_3$P compounds are metallic, with a pronounced Fe 3d component across the Fermi level. Our study provides the theoretical basis for the further investigation of Fe–P binary compounds. It is also important to explore the constituents of the Earth's core.

Acknowledgements

the calculations were performed in the High Performance Computing Centre of Jilin University.

Notes and references

1 J.-P. Poirier, *Phys. Earth Planet. Inter.*, 1994, **85**, 319–337.
2 A. S. Côté, L. Vačadlo and J. P. Brodholt, *Geophys. Res. Lett.*, 2008, **35**, L05306.
3 H. S. Washington, *Am. J. Sci.*, 1925, **53**, 352–378.
4 S. Ono, A. R. Oganov, J. P. Brodholt, L. Vočadlo, I. G. Wood, A. Lyakhov, C. W. Glass, A. S. Côté and G. D. Price, *Earth Planet. Sci. Lett.*, 2008, **272**, 481–487.
5 D. Errandonea, D. Santamaría-Perez, A. Vegas, J. Nuss, M. Jansen, P. Rodríguez-Hernandez and A. Muñoz, *Phys. Rev. B: Condens. Matter Mater. Phys.*, 2008, **77**, 94113.
6 N. Sata, K. Hirose, G. Shen, Y. Nakajima, Y. Ohishi and N. Hirao, *J. Geophys. Res.: Solid Earth*, 2010, **115**, B09204.
7 D. M. Sherman, *Earth Planet. Sci. Lett.*, 1995, **132**, 87–98.
8 W. F. Mcd, *Treatise Geochem.*, 2003, **2**, 547–568.
9 A. J. Stewart and M. W. Schmidt, *Geophys. Res. Lett.*, 2007, **34**, L13201.
10 G. Pratesi, L. Bindi and V. Moggi-Cecchi, *Am. Mineral.*, 2006, **91**, 451–454.
11 X. Wu, M. Mookherjee, T. Gu and S. Qin, *Geophys. Res. Lett.*, 2011, **38**, L20301.
12 H. P. Scott, S. Huggins, M. R. Frank, S. J. Maglio, C. D. Martin, Y. Meng, J. Santillán and Q. Williams, *Geophys. Res. Lett.*, 2007, **34**, L06302.
13 T. Gu, Y. Fei, X. Wu and S. Qin, *Earth Planet. Sci. Lett.*, 2014, **390**, 296–303.
14 P. Dera, B. Lavina, L. A. Borkowski, V. B. Prakapenka, S. R. Sutton, M. L. Rivers, R. T. Downs, N. Z. Boctor and C. T. Prewitt, *Geophys. Res. Lett.*, 2008, **35**, L10301.
15 T. Gu, X. Wu, S. Qin, C. McCammon and L. Dubroksky, *Eur. Phys. J. B*, 2013, **83**, 311.
16 X. Wu and S. Qin, *J. Phys.: Conf. Ser.*, 2010, **215**, 12110.
17 T. Gu, X. Wu, S. Qin and L. Dubrovinsky, *Phys. Earth Planet. Inter.*, 2011, **184**, 154–159.
18 H. Yan, *Comput. Mater. Sci.*, 2015, **107**, 204–209.
19 E. Dahl, *Acta Chem. Scand.*, 1969, **23**, 2677–2684.
20 T.-T. Gu, X. Wu, S. Qin, J. Liu, Y.-C. Li and Y.-F. Zhang, *Chin. Phys. Lett.*, 2012, **29**, 26102.
21 J. Wu, X. Chong, R. Zhou, Y. Jiang and J. Feng, *RSC Adv.*, 2015, **5**, 81943–81956.
22 P. F. McMillan, *Chem. Soc. Rev.*, 2006, **35**, 855–857.
23 Y. Wang, J. Lv, L. Zhu and Y. Ma, *Phys. Rev. B: Condens. Matter Mater. Phys.*, 2010, **82**, 94116.
24 Y. Wang, J. Lv, L. Zhu, S. Lu, K. Yin, Q. Li, H. Wang, L. Zhang and Y. Ma, *J. Phys.: Condens. Matter*, 2015, **27**, 203203.
25 A. P. Drozdov, M. I. Eremets, I. A. Troyan, V. Ksenofontov and S. I. Shylin, *Nature*, 2015, **525**, 73–76.
26 D. Duan, Y. Liu, F. Tian, D. Li, X. Huang, Z. Zhao, H. Yu, B. Liu, W. Tian and T. Cui, *Sci. Rep.*, 2014, **4**, 6968.
27 Y. Li, J. Hao, H. Liu, Y. Li and Y. Ma, *J. Chem. Phys.*, 2014, **140**, 174712.
28 Y. Li, J. Hao, H. Liu, S. Lu and J. S. Tse, *Phys. Rev. Lett.*, 2015, **115**, 105502.
29 L. Zhu, H. Liu, C. J. Pickard, G. Zou and Y. Ma, *Nat. Chem.*, 2014, **6**, 644–648.
30 W. Zhang, A. R. Oganov, A. F. Goncharov, Q. Zhu, S. E. Boulfelfel, A. O. Lyakhov, E. Stavrou, M. Somayazulu, V. B. Prakapenka and Z. Konopkova, *Science*, 2013, **342**, 1502–1505.
31 M. S. Miao, X. L. Wang, J. Brgoch, F. Spera, M. G. Jackson, G. Kresse and H. Q. Lin, *J. Am. Chem. Soc.*, 2015, **137**, 14122–14128.
32 D. Pinkowicz, M. Rams, M. Misek, K. V. Kamenev, H. Tomkowiak, A. Katrusiak and B. Sieklucka, *J. Am. Chem. Soc.*, 2015, **137**, 8795–8802.
33 F. Peng, M. Miao, H. Wang, Q. Li and Y. Ma, *J. Am. Chem. Soc.*, 2012, **134**, 18599–18605.
34 H. Wang, J. S. Tse, K. Tanaka, T. Iitaka and Y. Ma, *Proc. Natl. Acad. Sci. U. S. A.*, 2012, **109**, 6463–6466.
35 J. Botana, X. Wang, C. Hou, D. Yan, H. Lin, Y. Ma and M. S. Miao, *Angew. Chem., Int. Ed.*, 2015, **127**, 9412–9415.
36 L. Zhu, H. Liu, C. J. Pickard, G. Zou and Y. Ma, *Nat. Chem.*, 2014, **6**, 644–648.
37 X. Zhong, H. Wang, J. Zhang, H. Liu, S. Zhang, H. F. Song, G. Yang, L. Zhang and Y. Ma, *Phys. Rev. Lett.*, 2016, **116**, 57002.
38 Y. Wang and Y. Ma, *J. Chem. Phys.*, 2014, **140**, 40901.
39 Y. Wang, J. Lv, L. Zhu and Y. Ma, *Comput. Phys. Commun.*, 2012, **183**, 2063–2070.
40 J. Lv, Y. Wang, L. Zhu and Y. Ma, *Phys. Rev. Lett.*, 2011, **106**, 15503.
41 L. Zhu, H. Wang, Y. Wang, J. Lv, Y. Ma, Q. Cui, Y. Ma and G. Zou, *Phys. Rev. Lett.*, 2011, **106**, 145501.
42 M. Zhang, H. Liu, Q. Li, B. Gao, Y. Wang, H. Li, C. Chen and Y. Ma, *Phys. Rev. Lett.*, 2015, **114**, 15502.
43 S. Zhang, L. Zhu, H. Liu and G. Yang, *Inorg. Chem.*, 2016, **55**, 11434–11439.
44 G. Yang, Y. Wang, F. Peng, A. Bergara and Y. Ma, *J. Am. Chem. Soc.*, 2016, **138**, 4046–4052.
45 J. P. Perdew, K. Burke and M. Ernzerhof, *Phys. Rev. Lett.*, 1996, **77**, 3865–3868.
46 G. Kresse and J. Furthmüller, *Phys. Rev. B*, 1996, **54**, 11169–11186.
47 P. E. Blöchl, *Phys. Rev. B*, 1994, **50**, 17953–17979.
48 A. Jain, G. Hautier, C. J. Moore, S. Ping Ong, C. C. Fischer, T. Mueller, K. A. Persson and G. Ceder, *Comput. Mater. Sci.*, 2011, **50**, 2295–2310.
49 C. Rdl, F. Fuchs, J. Furthmller and F. Bechstedt, *Phys. Rev. B: Condens. Matter Mater. Phys.*, 2009, **79**, 235114.
50 A. Koumina, M. Bacmann, D. Fruchart, S. Niziol, P. Wolfers, M. Mesnaoui, J. Tobola, S. Kaprzyk, R. Zach and N. Techniques, *Ann. Chimie Sci. Materiaux*, 1998, **23**, 177–180.
51 M. Cococcioni and S. de Gironcoli, *Phys. Rev. B*, 2005, **71**, 35105.
52 J. D. Pack and H. J. Monkhorst, *Phys. Rev. B*, 1977, **16**, 1748–1749.
53 A. Togo, F. Oba and I. Tanaka, *Phys. Rev. B: Condens. Matter Mater. Phys.*, 2008, **78**, 134106.
54 R. Dronskowski and P. E. Blöchl, *J. Phys. Chem.*, 1993, **97**, 8617–8624.

55 R. Skála and M. Drábek, *Mineral. Mag.*, 2003, **67**, 783–792.

56 S. Rundqvist and F. Jellinek, *Acta Chem. Scand.*, 1959, **13**, 425–432.

57 N. Kohlhaas, R. Dunner and P. Schmitz-Pranghe, *Z. Angew. Phys.*, 1967, **23**, 245.

58 T. Takahashi, W. a. Basett and H.-K. Mao, *J. Geophys. Res.*, 1968, **73**, 4717–4725.

59 T. Sugimoto, Y. Akahama, H. Fujihisa, Y. Ozawa, H. Fukui, N. Hirao and Y. Ohishi, *Phys. Rev. B: Condens. Matter Mater. Phys.*, 2012, **86**, 24109.

60 H. Katzke and P. Tolédano, *Phys. Rev. B: Condens. Matter Mater. Phys.*, 2008, **77**, 24109.

61 J. F. Janak, *Phys. Rev. B*, 1977, **16**, 255–262.